Eur. Phys. J. D **10**, 379–390 (2000)

THE EUROPEAN PHYSICAL JOURNAL D

EDP Sciences

Rydberg states in the condensed phase studied by fluorescence depletion spectroscopy

F. Vigliotti and M. Chergui[a]

Institut de Physique de la Matière Condensée, Faculté des Sciences, Université de Lausanne, 1015 Lausanne-Dorigny, Switzerland

Received 28 July 1999 and Received in final form 8 November 1999

Abstract. Higher Rydberg states of NO trapped in rare gas matrices have been studied by inducing Rydberg-Rydberg transitions from the lowest $A^2\Sigma^+$ ($3s\sigma$) Rydberg state and detecting its fluorescence depletion. This technique unravels Rydberg states, which cannot be accessed by ground state absorption. However, no clear cut Rydberg series show up. The data show a compression of the n–$(n+1)$ splittings between Rydberg states, as well as of the $\ell\lambda$ splittings. The results are rationalised in terms of the quantum defect model and the lack of extended Rydberg series is due to the compression of high-n Rydberg states in a tiny energy region below the ionisation potential. Finally, fluorescence depletion data of NO trapped in amorphous sites (the so-called red sites) of solid Ar can be interpreted in terms of the gas phase NO–Ar van der Waals data. A general discussion on the fate of Rydberg states in van der Waals complexes, in liquids, and in solids is presented in an attempt to relate the data in these different media.

PACS. 31.50.+w Excited states – 31.70.Dk Environmental and solvent effects – 71.35.Aa Frenkel excitons and self-trapped excitons

1 Introduction

The fate of Rydberg states in condensed matter is still a matter of debate despite several studies over the past three decades. Rare gas media have mostly been used to investigate the spectroscopy of atomic and molecular Rydberg states in high-pressure gases [1–3], liquids [4–11], solids [11–23] and, more recently, in clusters [24–27]. These studies include photoabsorption [1–3, 6,9,11,13–15], photoconductivity [4–8], photoemission and photoelectron spectroscopy [11], and fluorescence-excitation spectroscopy [10–13,23–28]. The main feature, which determines the behaviour of Rydberg states in condensed phase media are their large orbital radii, which make them extremely sensitive to the presence of external perturbers. This property has even been used to distinguish between Rydberg and non-Rydberg states in the early days of molecular spectroscopy [1]. The extreme case of perturbation occurs, naturally, at solid state densities.

Absorption by Rydberg states has been studied in detail in the case of pure and rare gas-doped rare gas solids and a detailed review is given in reference [11]. A series of bands show up that have so far been interpreted in terms of Wannier excitons except for the lowest $n = 1$ member of the series. Wannier excitons represent bound electron-hole pairs with energies described by the well-known hydrogenic formula:

$$E_n^i = E_g^i - \frac{B_i}{n^2} \tag{1}$$

where

$$B_i = 13.6\left(\frac{m^*}{\varepsilon^2}\right) \tag{2}$$

is an effective Rydberg constant, which takes into account the dielectric shielding of the Rydberg electron by the crystal (ε) and the effective mass of the electron in the conduction band of the solid (m^*). In this picture, B_i is essentially independent of the nature of the dopant. n is the exciton main quantum number, and E_g^i is the impurity ionisation potential in the solid, expressed by:

$$E_g^i = I_g + P_+ + V_0 \tag{3}$$

where I_g is the gas phase impurity ionisation potential, P_+ is the polarisation energy of the medium by the positive ionic core and V_0 is the electron affinity of the medium.

Wannier excitons have no parentage with the free species excited states. However, the $n = 1$ exciton, whose radius is smaller than the unit cell, fails to be described by equation (3), which thus applies only for $n \geq 2$. The deviation for the $n = 1$ exciton is mainly ascribed to the so-called central cell correction [29]. Alternatively, the $n = 1$ exciton has been recognised as the lowest atomic Rydberg excitation, perturbed by the environment, which causes

[a] e-mail: majed.chergui@ipmc.unil.ch

a blue shift, and have thus been discussed as Frenkel excitons [30]. In order to get a unified picture of the absorption series, Dressler [31] and later Resca *et al.* [32] replaced equation (1) by a quantum defect modified series

$$E_n^i = E_g^i - \frac{B_i}{(n-\delta_n)^2}\cdot \tag{4}$$

The quantum defect δ_n, together with B_i, includes solid-state effects due to the surrounding atoms and the deviations from the Coulomb potential, due to the core, within a sphere around the central atom. δ_n in the matrix is different from the gas phase value. Basically, the quantum defect model supposes that the electron-hole interaction in the solid is the same as in the gas phase within a certain radius, and that it is a screened Coulomb potential outside it. The contribution of the impurity comes into play through the ionisation potential and the quantum defect δ for a given Rydberg series. It should be noted that in this approach, δ also depends on the solvent and contains together with B_i all solid state effects due to the surrounding, as well as deviations from the Coulomb potential due to the core embedded in the dielectric medium. Independently from this approach, the ionisation potential of any species embedded in a dielectric medium can be estimated by equation (3).

Use of equation (4) yields values of E_g^i and B_i different from those obtained by equation (1). Contrary to the Wannier model, the quantum defect model implicitly establishes a connection between the free species excited states and those observed in the solid. However, a clear-cut connection has only been attempted by Dressler for the case of solid Xe [31] and by Chergui *et al.* for the case of NO in Ne matrices [12]. Another model was proposed, based on the Hulthèn potential [22], which interpolates between the pure Coulomb potential at distances less than the cage radius and the screened Coulomb potential at larger distances, while predicting a finite number of states in the series. This model was successfully applied to the case of alkali atoms in rare gas matrices, but did not deliver satisfactory results in the case of matrix-isolated NO [12]. All these models represent phenomenological approaches to the problem and no rigorous theory has, to date, been proposed to settle the matter as far as pure and doped rare gas solids are concerned.

Regarding molecules in rare gas matrices, studies on C_2H_2 [17], $C_{10}H_8$ [18], CS_2, OCS [19], D_2 [16], H_2 [13], H_2O [14], HCl [15] only revealed the lowest Rydberg states, in general, as blue shifted molecular excitations. In the case of C_2H_4, C_6H_6 and CH_3I, higher excitations were, in addition, reported and were interpreted in terms of Wannier excitons [11,17]. This interpretation is questionable, as the collective character of excitons cannot be satisfied in the case of a doped rare gas solid. Furthermore, in these large molecules, the spectra are complicated by the overlap of valence and continuum absorptions with the Rydberg transitions and hinder a clear assignment of the bands. In order to address the issue of molecular Rydberg states in van der Waals solids, we undertook some years ago a systematic study of the simpler and Rydberg state-rich NO molecule trapped in Ne, Ar, Kr, Xe [12], N_2 [28] and H_2 [23] matrices. In Ne matrices, the $n = 3$ and $n = 4$ members of the Rydberg series were observed, with their associated $n\ell\lambda$ ($\lambda \leq \ell < n$), where ℓ is the electronic atomic angular momentum and λ its projection along the molecular axis. In the other matrices, only the $n = 3$ members could be observed. In all cases, no Rydberg series were found despite a careful search for higher members of the series. The quantum defect model (Eq. (3)) could not account for the observed vertical Rydberg transition energies, and especially, for the cut-off of the Rydberg series. However, we suggested that the cut-off of the vertical Rydberg series could be caused by the fact that the $n \geq 5$ states in Ne and the $n \geq 4$ states in the other matrices, have their vertical energies lying above the adiabatic ionisation limit and thus, are quenched to the ionisation continuum. In a recent calculation, Gross and Spiegelmann [33] have used a pseudo potential method to calculate the NO Rydberg absorption energies in a cluster of 140 Ar atoms. They have confirmed that when accessed from the ground state, the higher Rydberg states are shifted into the ionisation continuum, whose adiabatic energy is lower in the Ar environment as compared to the gas phase.

Since higher Rydberg states are difficult to access from the ground state, we recently proposed a fluorescence depletion technique aimed at accessing them from the lowest Rydberg state $A(3s\sigma)$, in equilibrium with its environment. In a preliminary report [34], we demonstrated the feasibility of the technique in the case of NO in Ar matrices, and found that indeed, additional states can be accessed that are not observed by absorption from the ground state. Nevertheless, just as in ground state absorption, no clear-cut infinite Rydberg series shows up. However, we showed that equation (4) could account for the Rydberg-Rydberg transition energies and that the lack of an infinite Rydberg series in matrices could be explained by the congestion of higher Rydberg states in a tiny energy domain. In the present contribution, we give a complete account of our results in Ne, Ar and Xe matrices. Given the ground state absorption data [12] and the many studies on NO–Rg van der Waals complexes over the past few years [35–38], we believe it represents an ideal system for addressing the fate of molecular Rydberg states in condensed matter.

In Section 2, we will recall the main results of our previous studies, which are of relevance for the experimental method based on the fluorescence depletion technique. In Section 3, we will present the experimental technique. In Section 4, we present our results in Ne, Ar and Xe matrices and in Section 5, we address our results in the light of the quantum defect model and of the data on van der Waals complexes. We finally discuss a general scheme for the description of Rydberg states in the solid phase and their connection to the liquid phase and to van der Waals complexes.

2 Methodology

The fluorescence from the lowest Rydberg state $A^2\Sigma^+$ ($v = 0$) level of NO has been shown to stem from two trapping sites in rare gas matrices: the so-called main and red sites [21]. The main site is due to NO trapped at a substitutional location of the lattice and is stable with respect to annealing. Its fluorescence is strongly Stokes shifted with respect to the absorption, and it lies at energies higher than in the gas phase. The Stokes shift is a signature of extensive lattice rearrangement: the matrix atoms are pushed away as a result of the Pauli repulsion between the extended Rydberg orbital and the closed-shell rare gas atoms. This repulsive interaction leads to the lattice rearrangement, the formation of a "bubble" around the excited molecule. Quantitative data about the process was extracted from an analysis of the absorption and emission line shapes based on the harmonic approximation and the configuration coordinate model, where the latter is the cage radius [21,23,39].

Red sites in Ar, Kr and Xe matrices are characterized by a quasi-continuous absorption with no clear-cut structures and an onset that is weakly blue shifted with respect to the gas phase. Their fluorescence bands are red shifted with respect to the gas phase. They probably stem from loose and amorphous sites and are likely due to formation of NO(A)–$Ar_{n\geq 1}$ (or –$Kr_{n\geq 1}$, –$Xe_{n\geq 1}$) van der Waals complexes with NO sticking to one or more rare gas atoms of the loose cage. In the case of Ne, red site fluorescence was attributed to hexagonal close packed (*hcp*) defects of the lattice, on the grounds that it has a well defined absorption and that its emission is blue shifted with respect to the gas [21].

Along the intramolecular coordinate, Rydberg states of NO have nearly parallel potential curves, converging to the first ionisation limit, while valence states have their equilibrium configuration at larger distances. This means that Rydberg-Rydberg transitions are dominated by $\Delta v = 0$ transitions and are therefore characterized by a single main band. On the other hand, along the intermolecular coordinate (which we take here as the radial distance from the NO impurity), this is not expected to be the case. The principle of the experiment is depicted in Figure 1, which schematically shows the intermolecular NO-matrix potentials in the configuration coordinate model and harmonic approximation. The idea is to access the higher Rydberg states from the cage minimum of the A-state intermolecular potential (*i.e.* after cage relaxation has been completed). We proceed as follows (see Fig. 1): a first laser excites the A-state from the ground state configuration (step I). This induces a relaxation of the cage around the excited molecule (step II). After a time delay ($\sim$ 20 ns), a second tunable laser probes the higher Rydberg states from the configuration of the relaxed A-state (step III). The detected signal is the depletion of the A-state fluorescence (step IV), its lifetime ranging from 150 to 450 ns in rare gas matrices [40].

The fluorescence depletion technique of the A-state of NO has already been implemented in the gas phase [41], but a charge detection (*e.g.* in resonant MPI [42]) gives much better signal-to-noise ratios. We tried to implement charge detection in the case of NO-doped rare gas solids but failed because of sample charging, and we resorted to the fluorescence depletion technique. The latter has, however, specific advantages over other techniques:

(a) it ensures that the initial state of the transitions is the $A(3s\sigma)$ state;
(b) it allows a site-selectivity, since the emission bands of the red and main site Rydberg fluorescence [21] can be well distinguished.

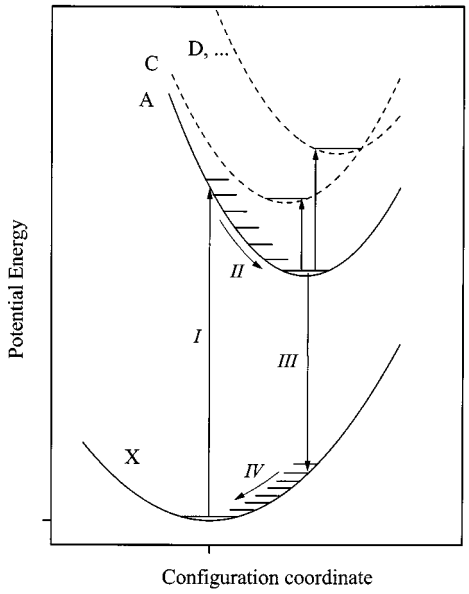

Fig. 1. Configuration coordinate model of NO in matrices in the harmonic approximation and principle of the experiment (see text). The configuration coordinate is the cage radius.

3 Experimental

The samples were grown by condensing a gaseous mixture of NO and the matrix species (typical dilutions of 3:1000) onto an MgF_2 window, cooled to temperatures ranging from 4 K to 25 K. In studying the main sites and in order to minimise the population of red sites in the case of Ne matrices, the samples were deposited at temperatures $\geq$ 7 K. This was necessary as the absorption bands of main and red sites both overlap with the excitation wavelength (193 nm) [21]. In the case of Ar or Xe, the excitation was more selective, and high temperature depositions were not necessary. Still, growing the samples at higher temperatures had no effect on the results. NO (99.5%), Ne (99.99%), Ar (99.9999%) and Xe (99.995%), were used without further purification, after checking that purifying the gases in a liquid nitrogen trap did not improve the results.

As mentioned above, the Rydberg absorption bands of matrix-isolated NO are blue-shifted and broadened as compared to the gas phase. The extent of these modifications is matrix-dependent. Table 1 lists the energy

Table 1. Maxima and *fwhm* for the $A(0,0)$ absorption band of NO in inert gas matrices together with the excitation energies and excitation schemes used in this work.

	sites	Absorption band		Excitation	
		maxima (eV)	*fwhm* (eV)	*energy* (eV)	scheme
gaz		5.48			
Ne	*main*	6.46	0.18	6.41	ArF laser line (193.3 nm)
	red	6.39	0.22	6.41	ArF laser line (193.3 nm)
Ar	*main*	6.36	0.12	6.41	ArF laser line (193.3 nm)
	red	5.6–6.2		5.90	210 nm (1st S of 193.3 nm)
Xe	*main*	5.88	0.083	5.90	210 nm (1st S of 193.3 nm)

at maxima and the *fwhm* (full width at half maximum) of the main and red site A–$X(0,0)$ absorption bands in all matrices of interest. In the case of Ne and Ar matrices, light at 193.3 nm from an ArF laser was used for excitation. In Xe matrices and for the red sites of Ar matrices, excitation at 210.2 nm was obtained by stimulated Raman shifting of the 193.3 nm beam in a Raman cell filled with H_2 at 6 bar. In the case of the main sites of NO in Kr matrices, we could not achieve the energy required for excitation, so that this matrix is not considered here. Fluorescence was dispersed by a 0.5-m monochromator equipped with a 1200 gr/mm grating and detected by a UV photomultiplier.

Scanning the Rydberg-Rydberg transitions was done by means of an Optical Parametric Oscillator, pumped by the third harmonic of an injection-seeded Nd:Yag laser. The OPO tuning range was 450–680 nm (signal wave) and 730–1680 nm (idler wave). The probe linewidth was 0.2 cm^{-1} spectral and 5 ns temporal. In the case of Ne matrices, the pump laser was operated at 20 Hz to enable correction for the fluctuations of the pump laser, as well as for the drop (over tens of minutes) of the NO fluorescence, caused by radiation damage. In the case of the more stable Xe matrices, both lasers were operated at a repetition rate of 10 Hz and shot-to-shot fluctuations of the ArF laser were recorded by a photodiode. In all cases, the probe laser was running at a repetition rate of 10 Hz for the Rydberg-Rydberg transition. The intensity of the OPO laser was also recorded by a photodiode, and the spectra were corrected for shot-to-shot fluctuations and for the wavelength dependence of the intensity. The PM photocurrent, and the signal of the photodiodes were analyzed by a gated boxcar averager. The OPO pulse was delayed 20 ns with respect to the ArF laser pulse to avoid temporal overlap between the pump and probe pulses. This ensured that Rydberg-Rydberg transitions were probed from a fully relaxed cage configuration in the A state.

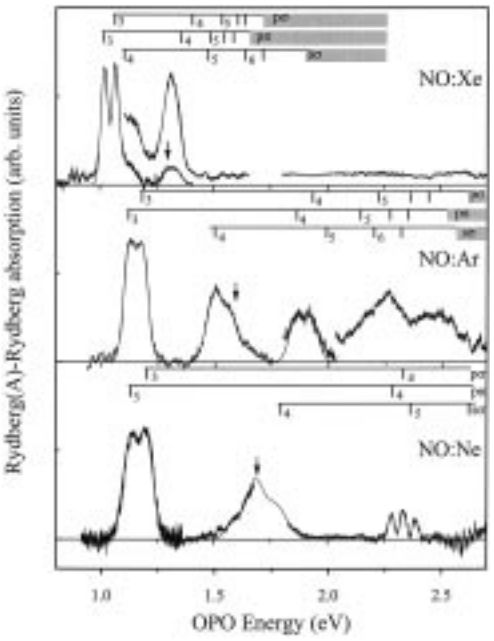

Fig. 2. Fluorescence depletion spectra of NO in Ne, Ar, and Xe matrices (main sites). The stick marks on top of each spectrum are the Rydberg series generated by equations (4, 5). The shaded area is the ionisation continuum in the matrix. Arrows denote the position of the d states included in the fits (all reported in Tab. 2). In the case of Xe, the upper trace between 1.1 eV and 2.7 eV was recorded at higher probe laser intensity.

4 Results

4.1 Main sites

Figure 2 shows the fluorescence depletion spectra of A ($v = 0$) in Ne, Ar and Xe matrices in the 0.9 to 2.7 eV range of the probe laser (there is a gap between 1.7 eV and 1.8 eV, due to the laser, see Sect. 3). In all matrices, one can distinguish two prominent bands around 1.1 eV, which are easily attributed to the A–C and A–D transitions (see below), followed by weaker bands containing some structures. The fluorescence depletion on the A–C/A–D bands was found to increase linearly with the intensity of the OPO laser up to a depletion level of 20 to 40%, depending on the matrix, beyond which it started to behave nonlinearly. An example is given in Figure 3 for the case of Ar matrices, where the A-state fluorescence level is shown as a function of the probe intensity set at the A–C transition. Fluorescence depletion being always weaker for all

Table 2. Energies of the $(n\ell\lambda)$ Rydberg states relative to the $A^2\Sigma^+$ $(3s\sigma)$ energy in the gas phase [43] and relative to the adiabatic energy $\left(E(3s\sigma)_{\rm zp}\right)$ [21] in the different matrices based on the present results.

			Gas	Ne		Ar		Xe	
state		$(n\ell\lambda)$	E–$E(3s\sigma)$ (eV)	E–$E(3s\sigma)$ (eV)	*fwhm* (eV)	E–$E(3s\sigma)$ (eV)	*fwhm* (eV)	E–$E(3s\sigma)$ (eV)	*fwhm* (eV)
C	$^2\Pi$	$3p\pi$	1.01	1.13	0.08	1.12	0.06	1.01	0.04
D	$^2\Sigma^+$	$3p\sigma$	1.13	1.20	0.07	1.18	0.06	1.06	0.04
E	$^2\Sigma^+$	$4s\sigma$	2.07	1.76	0.13	1.50	0.08	1.12	0.08
H	$^2\Sigma^+$	$3d\sigma$	2.29	1.59	0.08	1.57	0.06	1.29	0.05
H'	$^2\Pi$	$3d\pi$	2.3	1.68	0.08	1.61	0.13	1.33	0.05
K	$^2\Pi$	$4p\pi$	2.49	2.28	0.03	1.86	0.07	1.35	0.05
M	$^2\Sigma^+$	$4p\sigma$	2.54	2.33	0.03	1.93	0.07	1.40	0.04
S	$^2\Sigma^+$	$5s\sigma$	2.84	2.39	0.03	2.11		1.46	0.05
O	$^2\Sigma^+$	$4d\sigma$	2.95					1.53	0.05
O'	$^2\Pi$	$4d\pi$	2.95					1.59	0.05
Q	$^2\Pi$	$5p\pi$	3.23						
$E(3s\sigma)$[a] (eV)			5.48						
$E(3s\sigma)_{\rm zp}$[b] (eV)				5.90		6.00		5.70	

[a] Reference [43], [b] Reference [21].

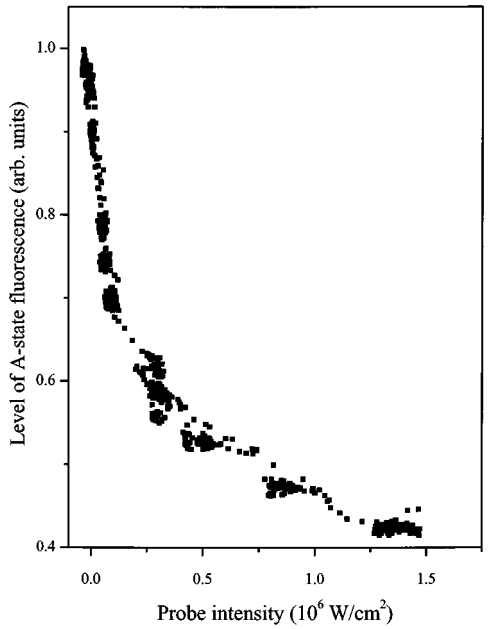

Fig. 3. Probe intensity dependence of the fluorescence depletion signal for the A–C transition of NO in Ar matrices.

the other bands, the spectra were corrected linearly for the intensity of the OPO laser, monitored by a photodiode.

The spectra in Figure 2 exhibit a number of characteristic features:

(i) the doublet structure around 1.1–1.2 eV;
(ii) a broader feature around 1.5–1.8 eV in Ne and Ar matrices, and around 1.3 eV in Xe matrices;
(iii) in Ne matrices, a distinct group of bands shows up around 2.3 eV and a continuous absorption without a clear structure is found above 2.5 eV;
(iv) in Ar matrices, a doublet structure appears at ~ 1.9 eV. Upon increasing the probe laser intensity by a factor of ~ 5, broad features appear at energies > 2 eV;
(v) in Xe matrices, no structures could be found above 1.5 eV and the fluorescence level remains unaffected up to ~ 2.5 eV (Fig. 2c). When increasing the OPO laser intensity, the depletion level increases but remains constant throughout the energy domain, while no new structures appear.

The gas phase energy splittings of the lowest Rydberg states of NO with respect to the A state, are given in Table 2. As discussed in reference [34], the structures at energies above 1 eV have to be attributed to transitions to higher Rydberg states of NO (Tab. 2) but it can be seen in the spectra that they occur at lower energies, as compared to the gas phase. This already suggests a compression of the Rydberg series in matrices. This is especially true, considering that the adiabatic (zero-phonon) energies of the A-state (given in Tab. 2) are greater than the gas phase energy.

In the gas phase, transitions from the A state to the C, D, H, H', K and M states have been observed [41–44]. The s–d transition to the F state is forbidden by the $\Delta\ell = \pm 1$ and $\Delta\Lambda = \pm 1$ selection rules. In the case of H and H', transitions become allowed due to $s \sim d$ mixing [44]. However, these mixings are determined by the energetics and intramolecular couplings specific to the gas phase. The situation is dramatically different in matrices and may also vary from matrix to matrix. It could lead either to an enhancement or a weakening of the mixings. Furthermore, many instances exist of a relaxation of the $\Delta\Lambda \neq 2$ selection rule for electric dipole transitions because of the local site symmetry in matrices, and in the case of NO in particular [45]. In order to establish the

connection between the features observed in Figure 2 and the gas phase Rydberg-Rydberg transitions, we have adopted the following guidelines.

(a) Energy splittings within a given $(n\ell\lambda)$ complex (for a fixed n) should remain of the same order of magnitude as those of the gas phase. This is reasonable since the $\ell\lambda$ splittings result from the projection of the orbital momentum ℓ onto the intramolecular axis and are therefore a property of the molecule. However, deviations are expected as each type of state ($s\sigma$, $p\sigma$, $p\pi$, ...) has a specific polarisability which determines its interaction with the environment. This was actually verified in the ground state absorption spectra where the gas-to-matrix shifts scaled down in the sequence $s\sigma$–$p\sigma$–$p\pi$ [12], because of the increase in attractive contributions.

(b) $n - n'$ $(n' > n)$ splittings may substantially be affected by the medium. This is reasonable, since in going from $n = 3$ states, where the orbital extension is of the order of the nearest neighbour distance, to $n > 3$ states, the Rydberg orbital encompasses the first shell (or beyond) of matrix atoms. The concurrent effects to such a situation are that:

(i) the electron density at a given point decreases, and so do the repulsive interactions too and,
(ii) the ionic core is less shielded and the polarisation contributions increase, leading to an increase of the attractive contributions in the energy balance. Furthermore, this effect should increase with the polarisability of the matrix.

(c) Finally, the integrated intensities of the bands were considered for consistency in each matrix by setting the intensity of the A–C transition to unity and comparing the relative intensities to the gas phase ones. This criterion should apply for allowed transitions. Indeed, we noted that the relative intensities of the ground state absorption to the A, C and D states are conserved in matrices [12].

The spectra in Figure 2 were fitted with Gaussian line shapes. The band maxima and widths resulting from the fits are listed in Table 2 and the relevant energy splittings are compared with those obtained from the ground state absorption spectra of NO in matrices as well as with the gas phase splittings.

It is straightforward to assign the doublet structure below 1.2 eV to the $A(3s\sigma)$–$C(3p\pi)$ and $A(3s\sigma)$–$D(3p\sigma)$ transitions on the basis of the gas phase data (energies and intensities). As anticipated, the $s\sigma$–$p\sigma$–$p\pi$ splittings are not strictly identical to those of the gas phase but are mildly matrix-dependent (Tab. 2).

For the assignment of the higher energy structures, the $n \geq 4$ and the $3d$ states have to be invoked. In this latter case, both $\Delta\Lambda$ and $\Delta\ell$ selection rules come into play but, as mentioned above, matrix effects on both the energetics and the symmetry may make their appearance in the spectra matrix-dependent.

Given that the case of Ar matrices has already been discussed [34], we briefly recall the main conclusions concerning it. We identified the bands at 1.51, 1.87 and 1.91 eV as the A–$E(4s\sigma)$, A–$K(4p\pi)$ and A–$M(4p\sigma)$ transitions, respectively, on the basis of:

(i) the energy ordering of the states (see Tab. 2);
(ii) the fact that the energy splittings between the $4\ell\lambda$ states, $E(4s\sigma)$, $K(4p\pi)$ and $M(4p\sigma)$ are only slightly different to those of the gas phase (Tab. 2). On the other hand, this assignment implied a drastic reduction (by ~ 0.5 eV) of the $(n = 3)$–$(n = 4)$ splitting, in agreement with point (b) above;
(iii) the structures which appear in the shoulder of the 1.5 eV band (shown by an arrow in Fig. 2) were assigned to the A–$H(3d\pi)$ and A–$H'(3d\sigma)$ transitions, as these are the only possible candidates left (Tab. 2). This assignment implies however that the s–d splitting within the $n = 3$ states is drastically reduced in Ar matrices as compared to the gas phase. This conclusion is not unrealistic as d-states have near-zero quantum defects and therefore do not efficiently shield the core. In such a case, the polarisation contributions of the latter are important and lead to a strong reduction of the energy of the state;
(iv) the broad structure above 2 eV has been assigned to higher members of the Rydberg series, which are highly compressed just below the ionisation limit. These higher Rydberg states were estimated using equation (4) (see also Sect. 5).

In the case of Ne matrices and on the basis of point (c) above, we would expect the $(n = 3)$–$(n = 4)$ splitting to be larger than in Ar since Ne is a less polarisable matrix. This is actually the case if we consider now that the broad structure around 1.6 eV is the analogue of the 1.5 eV band in Ar, even though only the wings could be recorded. It is however clear that it contains more than one structure if we compare it to the bands that show up at higher or lower energies. Adopting the same assignment as in Ar, we find that the splitting is now 1.6–1.8 eV, indicating a compression of the Rydberg series in Ne matrices, as compared to the gas phase, but less important than in Ar matrices. If we attribute the bands at 2.28 and 2.33 eV to the $K(4p\pi)$, $M(4p\sigma)$ states and assume that their splitting with respect to the E state is nearly the same as in the gas phase, the E state falls at 1.765 eV, thus comforting the analogy with the Ar matrix. The band at 2.39 eV is then attributed to the $5s\sigma$ state, which is the only choice left. This assignment confirms that the compression of the Rydberg series becomes increasingly important, the higher we climb the Rydberg ladder. A feature that is expected on the basis of point (b) above.

In the case of Xe matrices, the A–C and A–D energy splittings exhibit a further reduction as compared to Ne and Ar matrices. Indeed the polarisability of the matrix is higher and therefore the attractive contributions too. As far as the $(n = 3)$–$(n = 4)$ splitting is concerned, we expect it to be significantly more reduced than in Ar matrices, and we tentatively assign the shoulder at ~ 1.1 eV to the $E(4s\sigma)$ state. This implies an $(n = 3)$–$(n = 4)$ splitting reduced by ~ 1 eV as compared to the gas phase. A possible choice for the broad band at 1.3–1.4 eV is to attribute it to transitions to the K and M states, despite an $\ell\lambda$ splittings which is further reduced as compared

Table 3. $\ell\lambda$, n–$(n+1)$ and λ-energy splittings between the Rydberg states of NO in the gas phase and main sites. $\Delta E(n = 3$–$n = 4)$ is the gas-to-matrix difference of the $n = 4$ to $n = 3$ energy splitting.

		ΔE (eV)			
		gas	Ne	Ar	Xe
fixed n	$3p\pi$–$3s\sigma$	1.01	1.13	1.12	1.01
	$3p\sigma$–$3s\sigma$	1.13	1.20	1.18	1.06
	$3d\sigma$–$3s\sigma$	2.29	1.59	1.57	1.29
	$3d\pi$–$3s\sigma$	2.30	1.68	1.61	1.33
	$4p\pi$–$4s\sigma$	0.42	0.51	0.36	0.24
	$4p\sigma$–$4s\sigma$	0.47	0.57	0.43	0.28
fixed n, ℓ	$3p\sigma$–$3p\pi$	0.12	0.07	0.06	0.05
	$4p\sigma$–$4p\pi$	0.05	0.05	0.07	0.05
	$3d\pi$–$3d\sigma$	0.01	0.09	0.04	0.04
	$4d\pi$–$4d\sigma$				0.05
fixed ℓ, λ	$4p\pi$–$3p\pi$	1.48	1.15	0.73	0.34
	$4p\sigma$–$3p\sigma$	2.54	2.33	1.93	1.40
	$4s\sigma$–$3s\sigma$	2.07	1.76	1.50	1.12
	$5s\sigma$–$4s\sigma$	0.77	0.62	0.61	0.34
$\Delta E(n = 4$–$n = 3)$	$s\sigma$		−0.31	−0.57	−0.95
	$p\pi$		−0.33	−0.75	−1.14
	$p\sigma$		−0.28	−0.67	−1.07

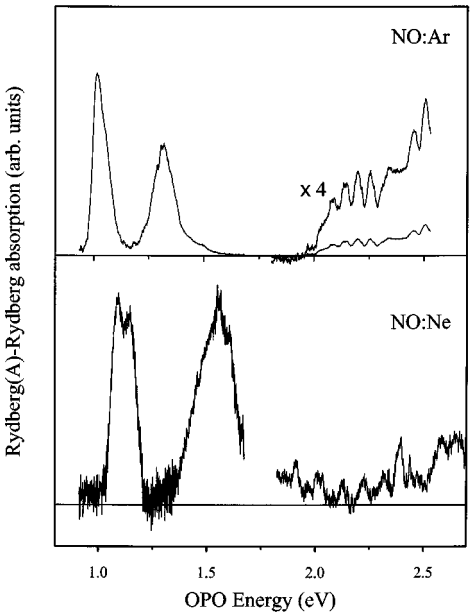

Fig. 4. Red site fluorescence depletion spectra in Ne and Ar matrices. The Ne spectrum has not been corrected for the probe laser intensity.

to Ar matrices, and this would be consistent with the trend observed in the case for the $3\ell\lambda$ states (Tab. 3). Another choice is to attribute it to $3d$ states ($3d\pi$, $3d\sigma$), as in Ar matrices. In fact, we propose that the band at 1.3–1.4 eV consists of all four contributions, with the $3d$ states lying below the $4p$ ones. The weak structures in the 1.4–1.6 eV are probably due to $n \geq 5$ members of the Rydberg series as will be shown below. Finally, at higher energies, the constant depletion signal that shows up at high probe laser intensity suggests that we are probably in the conduction band of the solid. Indeed, the ionisation potential of NO in Xe matrices is around 7–7.5 eV [12]. Since the adiabatic energy of the A state is 5.7 eV [21], the ionisation continuum is reached for energies of the probe laser ≥ 1.3 eV.

Table 3 summarises the data of Table 2 in terms of n-, ℓ-, and λ-splittings. From Tables 2 and 3 and from Figure 3, we infer the following trends.

(a) Higher members of the Rydberg series of NO are observed which could not be detected by vertical excitation from the ground state [12].
(b) A one-to-one correspondence can be established with the gas phase spectrum, at least for principal quantum numbers up to $n = 5$, but higher-n Rydberg states are not clearly distinguished.
(c) The energy separation between $n = 3$ and $n > 3$ states shows a compression of the Rydberg series which increases by almost a factor of 2 in the sequence gas–Ne–Ar–Xe.
(d) The initial assumption of a nearly conserved $\Delta\ell$ splitting breaks down in the heavier matrices and for higher-n states.
(e) s–d splittings are far more reduced in matrices than s–p splittings. This is explained in terms of the near-zero quantum defect of the d-series implying almost no shielding of the NO^+ core by the electron. This leads to important polarisation contributions of the core in the dielectric medium. As a consequence, the s–d transition energy decreases, leading to a smaller energy splitting than in the gas phase. In this respect, it is interesting to note that according to our assignment, the $3s\sigma$–$3d\sigma$ splitting decreases by 0.722 eV compared to its gas phase value, while the polarisation contribution calculated by Gross and Spiegelmann [33] amounts to 0.761 eV. It should however be mentioned that their calculation was carried out at the ground state equilibrium configuration of NO in Ar matrices.

4.2 Red sites

Figure 4 shows the fluorescence depletion spectra of NO in Ne and Ar matrices. As in the case of the main sites, they are characterized by a doublet structure around 1 eV, followed by a broad structure at 1.5 eV and 1.3 eV in Ne and Ar, respectively. Above 1.8 eV in Ne and 2 eV in Ar, several sharp bands appear. In Ne, they can be grouped in a progression with a spacing of 810 ± 50 cm^{-1} up to 2.4 eV. Above 2.4 eV, this progression overlaps with additional bands and a regular progression is more difficult to distinguish. In Ar matrices, the bands are spaced by about 460 cm^{-1}, superimposed on a continuous background at ~ 2 eV above the A-state energy. In Ne and Ar, the structures at ~ 1.1 eV bear strong resemblance with their main sites counterparts and are probably due to the C and D states.

Table 4. Analysis of the main sites data using equation (5). The values for the quantum defect are those of the gas phase (see text).

series				$s\sigma$		$p\pi$		$p\sigma$		
gas				$\delta = 1.18$		$\delta = 0.75$		$\delta = 0.7$		
	$\varepsilon^{(a)}$	$P_+ + V_0{}^{(b)}$	E_g^i	E_g^i	B_i	E_g^i	B_i	E_g^i	B_i	$B_i(m^* = 1)$
		(eV)		(eV)		(eV)		(eV)		(eV)
gas	1			9.26						
Ne	1.24	0, +1.98	> 9.26	9.1	10.0	9.3	11.2	9.4	11.6	8.8
Ar	1.66	−0.75, −1.17	8.3 ± 0.2	8.6	8.5	8.5	7.1	8.6	7.7	4.9
Xe	2.22	−1.79, −2.23	7.26 ± 0.22	7.6	6.3	7.4	3.3	7.4	3.5	2.8

(a) Reference [32], quoted from L. Resca, S. Rodriguez, Phys. Rev. B **17**, 3334 (1978),
(b) values of the literature summarized in reference [12].

5 Discussion

The discussion is divided in three parts. We first address the case of the main site transitions, then we discuss the red sites. The third part concerns a general discussion on Rydberg states in solids, liquids and van der Waals complexes and the connection between these different media.

5.1 Main sites

In reference [34], equation (4) was used to describe the Rydberg-Rydberg transitions of NO in Ar matrices. It yielded satisfactory results in that the derived ionisation potential agreed with that obtained with equation (3), and that it could account for the lack of higher Rydberg states. Since it is a continuum approximation, one might question its applicability in our case, where absorption starts off from a cage relaxed configuration in the excited state. We believe it is still a good approximation in this case as: (a) even though the A-state is in a relaxed configuration, the blue shift in emission still points to a penetration of its wavefunction into the medium; (b) the radius of the Rydberg orbital increases by a factor of ~ 2.4 in going from $n = 3$ to $n = 4$ (the radius of the center of gravity of the electron cloud scales as $(1/2)\big(3n^{*2} - \ell(\ell+1)\big)a_0$, where $n^* = n - \delta$, a_0 is the Bohr radius and δ the quantum defect [46]). Since the A-state equilibrated cage has a radius of ~ 4 Å, the $4s\sigma$ orbital encompasses the first shell of atoms, even in its A-state relaxed configuration. Use of equation (3) rests on a knowledge of B_i, which is known for crystals in their ground state configuration. It is expected that it will probably differ in the equilibrated excited solid. Furthermore, quantum defects measure the extent of the penetration of the Rydberg electron in the core [46], and will be fixed at their gas phase value. Thus, from the value of the n–$(n+1)$ energy splittings reported here between Rydberg states, we can generate a Rydberg series keeping the effective Rydberg constant as adjustable parameter. The result of the fitting procedure is shown in Figure 2 and summarized in Table 4 and the following trends are noted.

(a) In all cases, the effective Rydberg constant derived from the fit is smaller than that of the gas phase and decreases in going from Ne to Xe matrices. While the value is roughly constant (within about 1.5 eV) for all series in Ne and Ar, in Xe matrices the value derived for the $s\sigma$ series is about twice as large as that derived for the $p\pi$ and $p\sigma$ series. We also give in Table 4 the value of B_i derived from equation (2). It can be seen that our fitted values are significantly larger. This can be explained by the fact that the spectra are recorded from a looser cage than that of the ground state. Screening by the matrix atoms and the effective mass approximation are less pronounced than starting from the ground state configuration, for which equation (2) is, in principle, valid. The large discrepancy between the B_i value for the $s\sigma$ states and the $p\pi/p\sigma$ states in Xe could be caused by the strong polarisation effect of these orbitals on the highly polarisable Xe matrix.

(b) From the adiabatic (zero-phonon, $E_{\rm zp}$) energy of the $A^2\Sigma^+$ $(v = 0)$ [21,39], we can now estimate the ionisation potential of NO in matrices using equation (4), where $E^i_{\rm zp} = E^i_{n,{\rm zp}}$ $(n = 3)$ and δ are given in Table 4 along with the derived B_i values. E_g^i is also independently determined by equation (3). In principle, these values should be close, provided the V_0 and P_+ values (used in Eq. (3)) represent the adiabatic energy of the free electron and of the polarisation contribution, respectively. The values obtained by these two estimates are compared in Table 4 and the agreement is satisfactory (within their uncertainties).

(c) With the values of E_g^i, δ and using equation (4), we have also generated the higher members $(n \geq 5)$ of the Rydberg series. Their positions are indicated in Figure 2 by sticks, while the ionisation continuum is shown as shaded bars. It is clear that these higher members are squashed in a tiny energy range of about 0.3 eV below the ionisation limit. This, together with the fact that the bands are broad, will give rise to a quasi-continuous absorption making a clear-cut assignment of individual members almost impossible. We therefore assign the continuous absorption above ~ 2.5 eV to absorption by the $n \geq 6$ members of the $s\sigma$, $p\pi$ and $p\sigma$ series in Ne matrices, and above 2.2 eV and 1.4 eV $n \geq 5$ members in Ar. In Xe matrices, the weak bands found above 1.4 eV are probably due to $n \geq 5$ members of the Rydberg series.

Thus, the use of the quantum defect formula, assuming gas phase quantum defects, gives a consistent picture of the Rydberg transitions of our spectra, and of the

non-observation of infinite Rydberg series. However, it is a phenomenological approach and the physical meaning of the derived effective Rydberg constants still needs to be clarified.

In reference [34], we adopted a somewhat different approach, in which we used the quantum defects as adjustable parameter, while keeping B_i fixed. The general conclusions from this approach are identical to the present ones, *i.e.* the non-observation of higher members of the series and the values of the ionisation potential are accounted for. It nevertheless suffers from two disadvantages. In the first place, the values of B_i reported in the literature are quite scattered, depending on both the method used to measure them and/or the way they were calculated [11,31,32]. Secondly, the quantum defects derived from the fits (we also repeated the calculations in the case of Ne and Xe matrices) are systematically larger than those of the gas phase. This contradicts the original picture of the quantum defect model [32], in which the matrix atoms introduce additional screening of the core against the Rydberg electron. This implies that the quantum defects should be smaller than in the gas phase as the extent of the penetration of the Rydberg orbital into the core is further reduced.

In conclusion, the quantum defect model accounts for the observation but it is a purely phenomenological approach, and a sound theoretical basis is called for to fully account for our results. In particular, it should provide a clear description of the interaction of the Rydberg electron with its surrounding both in its radial and angular parts.

5.2 Red sites

In Ar matrices, the red site fluorescence is shifted by ~ -50 meV with respect to the gas phase [21], suggesting the formation of a stable bond with atoms of the matrix. A detailed analysis of the spectroscopic data on the NO–Ar van der Waals complex was performed on the basis of *ab initio* NO^*–Ar potential surfaces [38]. It turns out that the spectroscopy of the NO(A)–Ar complex can be fairly well understood in terms of a single anisotropic potential surface with a shallow minimum on the oxygen side. It becomes substantially more complicated in the region of the $C(3p\pi)$ and $D(3p\sigma)$ states. In the presence of an Ar atom and in the C_s symmetry of the complex, the C state undergoes a Renner-Teller splitting of up to about 4000 cm^{-1} into A' and A'' states, while the D state correlates to an A' state in the complex. Mixing between the A' (C) and A' (D) components occurs at certain configurations, leading to a complicated vibrational structure.

At the minimum configuration of the NO(A)–Ar complex, which occurs at 180° and at an NO–Ar distance of 4.15 Å, the well depth is ~ 10 meV [38]. This is smaller than the 50 meV red shift reported in matrices [21]. However, in this latter case, even though we do not know the contribution of the ground state, we believe it is negligible at a distance of 4.15 Å. On the other hand, contributions from additional Ar atoms may add up to give the solvation energy of 50 meV in the excited state. We therefore suggest that in the amorphous sites, the impurity is in a loose cage and binds to several Ar atoms, without however forming a symmetric shell around it.

In the following, we will consider that adding more Ar atoms to the complex merely shifts the absolute energies of all the states but not their relative positions. This hypothesis is borne out by the results concerning the main sites where the relative positions of the states, although different from the gas phase, are not dramatically altered. If we consider the potential surfaces of the NO–Ar complex [38], we find that from the equilibrium configuration of the A-state in the complex, one accesses favourably both the C (A'') and $C + D$ (A') states by vertical excitation at 0.99 eV. This could be the main band, which appears in Figure 4. There is a less favourable transition to other configurations of the $C + D$ (A') state between 1.03 and 1.1 eV, which could be related to the blue wing of the main band in Figure 4. Finally, a broad band should show up above 1.2 eV, which is the limit of the potential curves given in reference [38]. This additional band is also due to the $C + D$ (A') state and probably corresponds to the broad band centered at 1.3 eV in our spectrum. This comparison between the data on the van der Waals complex and the red site data, supports the idea that the latter is due to van der Waals complexes, although with maybe more than one rare gas partner and in a non centrosymmetric configuration. Some similarities between the main features in Ar and in Ne matrices, would also point to a van der Waals complex origin in the latter case too. However, a number of points speak against such a hypothesis:

(a) the red site fluorescence in Ne matrices is blue shifted with respect to the gas phase,
(b) Ne matrices are self annealed and would tend to suppress amorphous sites,
(c) red site Rydberg absorption exhibits symmetric Gaussian absorption bands contrary to other matrices which showed a quasi-continuous structureless absorption band, characteristic of a distribution of sites [21].

For these reasons, we suggested that red sites in Ne are due to NO at an *hcp* site of the lattice [21]. Thus, the broad band at ~ 1.5 eV in Ne matrices could be due to the higher Rydberg H, H' and S states, just as in the case of the main sites, although a more detailed assignment is not attempted here.

Finally, concerning the higher energy sharp bands in Figure 4, we rule out that they can be due to the NO^+–Ar potential as its vibrational modes are of the order of 50 to 100 cm^{-1} [35,47]. The same holds in the case of Ne matrices. They are most likely due to valence states, which should also exhibit vibrational progressions. In Ne, the progression of bands spaced by 810 ± 50 cm^{-1} is tentatively attributed to transitions to high vibrational levels ($v > 20$) of the $B^2\Pi$ state, where the vibrational spacing is of about 800 cm^{-1}. In Ar, the bands are spaced by about 460 cm^{-1}. In this energy range (8.2 eV above the ground state), the B state has a vibrational energy spacing of typically 670 cm^{-1}. Therefore, it seems rather

unlikely that it be responsible for the observed progression. The other candidate would be the $b^4\Sigma^-$ state. It is less favourable from the point of view of selection rules, but has larger Frank-Condon factors with the A ($v = 0$) level than the B state.

Coming now to the continuous background above 2 eV in Ar, it could be attributed to the onset of the ionisation continuum. If the spectrum is compared with that of the main site, it seems possible that the ionisation continuum is red shifted with respect to that of the main site. In Ne, the onset of the ionisation continuum can tentatively be placed between 2.5 eV and 2.7 eV, where additional, larger structures appear. More studies would be needed to confirm the conclusions presented here. In particular a charge detection scheme could probably help distinguish the Rydberg states from the non-Rydberg ones, and work is in progress to develop such an experiment.

5.3 Rydberg states in van der Waals complexes, in liquids and in solids

From our work in solid matrices [12–15,21,23,28,39,40] and that of others in rare gas liquids [1–9] and in van der Waals complexes [35–38,47–50], it is possible draw some general trends as to the behaviour of Rydberg states in different states of matter, if one makes abstraction of fine details such as configuration interaction in the complex, as observed in the case of NO–Ar [38]. The behaviour of Rydberg states in dense rare gases can be grouped in different categories. These depend on the density and nature of the environment (solid or liquid), on the orbital quantum number ℓ (*i.e.* the shape of the orbital), and on the principal quantum number n. The latter determines the spatial extent of the orbital. Typical internuclear distances are of the order of a few Å in fluids and solids.

In fluids

Observations suggest two regimes characterized by whether the Rydberg states have high-n or low-n (*i.e.* also low ℓ) values. As a function of density, low-n states ($n \leq 5$) and low-ℓ ($\ell = 0, 1$) states exhibit in general either a weak red shift or no shift at all at moderate densities (typically 5×10^{21} cm^{-3}), while a further increase of density leads to a blue shift that increases to higher energies with increasing density. Eventually, it reaches the matrix values at solid state densities. Examples of this behaviour are given by NO [5] or Xe [9] in fluid Ar. These states have orbital radii that are of the order of the nearest neighbour distance at high densities and, due to their low ℓ values, they shield relatively well the core. At low densities, the interaction between the Rydberg excited species and the perturbers is dominated by long-range dispersive forces. As the density increases, the overlap of the Rydberg cloud with the perturbers increases, leading in general, to a positive (repulsive) energy contribution because of Pauli repulsion between the Rydberg electron and the closed shell rare gas species.

Coming now to high-n ($n > 5$) states, their radii are such that their orbitals can embed several solvent species. In this case, the energy of the excited species-solvent system can be described in terms of the Fermi model [51,52] or the improved model of Alekseev and Sobel'man [6,53, 54], in which the free electron energy and the core polarisation contributions act independently (as in Eq. (3)). In most rare gas media (except He and Ne), these contributions are negative at fluid densities [11]. This leads to a lowering of the Rydberg transition energies for absorption from the ground state, as indeed observed, *e.g.* in the case of the $n \geq 8$ d- and d'-states of CH_3I [4,6] and of the $n \geq 5$ states of C_6H_6 in fluid Ar [8]. In addition, the red shifts of the high-n Rydberg states with density have been found to be, in general, similar to that of the ionisation potential of the molecule [4,6,8].

Thus, for a given range of rare gas densities, the general trends will be that low-n Rydberg states shift blue with respect to the gas phase, while high-n and the ionisation potential shift red, thus leading to a compression of the Rydberg series.

In solids

For low-n states, as mentioned above, the impurity-environment interaction is largely dominated by repulsive contributions and the transition energies shift to the blue, as observed in all the cases so far reported [1,11–23]. The decrease of the n–$(n + 1)$ splitting which we report here suggests a compression of the Rydberg series, but no clear Rydberg series is observed. We believe that in going from a state of given (low) n to a higher-n states, the change of configuration in the solid is so drastic, that the transition probability drops dramatically. This change would be one in which we jump from a configuration where the electron does not fully penetrate the medium to one where it encompasses several medium species. Such drastic changes of configuration thus hinder the observation of extended Rydberg series.

Studies on van der Waals complexes [35–38,47–50] suggest a general picture of the interaction between a Rydberg excited species and a rare gas environment. For example, a systematic study of the interatomic potentials of singlet s Rydberg states of the Hg–Ne complex shows a clear change of regime as a function of main quantum number n ($n = 7$–10) [48]. Crossed molecular beam studies [49] also suggest a similar behaviour. This change of regime as a function of n for s-type Rydberg states is schematically depicted in Figure 5 and can be summarized as follows.

(a) For low-n states, the molecule-rare gas interaction is mildly attractive at large internuclear separations (*i.e.* with respect to the ground state configuration) and of van der Waals nature. At short distances, it is mainly repulsive because of Pauli repulsion and because the core is effectively shielded by the Rydberg electron. This leads to a potential curve that has a minimum at large distances compared to the ground state as has clearly been demonstrated in the case of the NO(A)–Rg complexes [35–38].

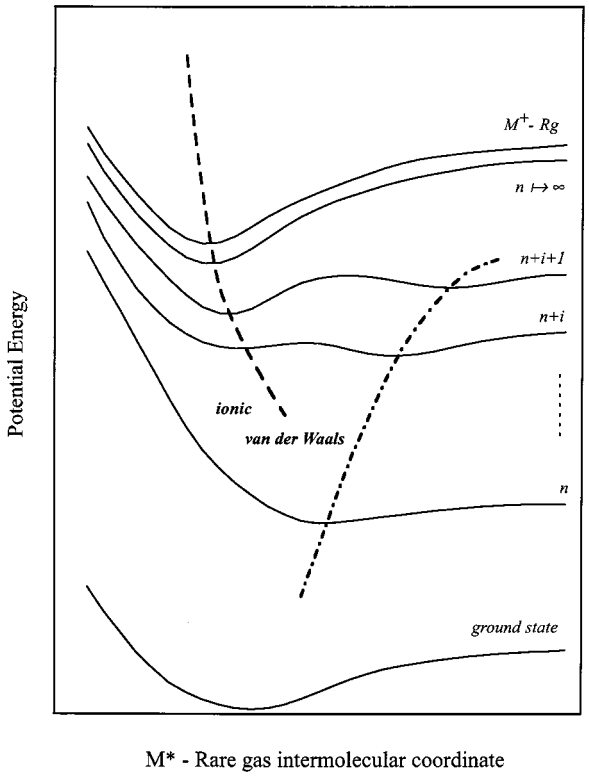

Fig. 5. Schematic diagram of the M^*–Rg interaction, where M^* is a Rydberg excited molecule.

(b) For intermediate-n states, the orbital radius increases and the electron density, at a given point, decreases. The long-range attractive van der Waals interaction is still present but it is weaker and lies at larger internuclear separations. At shorter distances, there is a small repulsive barrier due to weak Pauli repulsion and at even shorter distances, the interaction becomes attractive again because polarisation effects due to the positive ionic core come into play. This leads to a potential with a double minimum, one at large internuclear distances mainly due to the van der Waals part of the interaction, and one at short distances mainly due to the ionic part. The importance of both depends on the main quantum number and on the rare gas partner.

(c) For large n values, the orbital radius is very large and the electron density along the orbital is very low. The interaction is dominated by the polarisation energy of the positive ionic core, and consequently, the intermolecular potentials of the complex converge to those of the ionic complex.

We believe that this change of interaction regime as a function of n in the complexes is also operative in dense media where low-n (low-ℓ) states are blue shifted while high-n ones are red shifted [1–9]. In solid media, the non-observation of states of higher n is, as mentioned above, due to the drastic change of configuration, which occurs during the transition (Fig. 5). In this respect, it is interesting to note that in the case of the NO–Ne complex in the $E(4s\sigma)$ state, it has been suggested that the vibrational structure is close to that of the NO^+–Ne complex [37]. Finally, the picture outlined above may also provide a link between the molecular description and the quantum defect one in solids. Recently, the multichannel quantum defect theory (MQDT) has been extended to describe the interaction between a Rydberg excited species (NO) and a rare gas atom [47, 55]. The idea was that starting off from a potential surface of the NO^+–Ar and NO($3p\pi$)–Ar complexes, and using the Rydberg formula, one can construct a quantum defect surface, which depends on the Jacobian coordinates of the complex. This gives the deviation of the quantum defect in the complex as compared to the diatom. With this, it is possible to construct higher members of the $p\pi$ series in the complex [55]. It would be very interesting to compare and possibly relate the MQDT approach to the quantum defect model applied here for the Rydberg absorption in rare gas matrices.

6 Summary

A fluorescence depletion technique has been applied to study higher Rydberg states in the condensed phase, using the NO molecule in rare gas matrices as model system. It is found that more Rydberg states can be accessed by this technique than upon vertical excitation from the ground state. However, the bands are broad, pointing to an extensive rearrangement of the lattice cage around the Rydberg electron upon transition from one Rydberg state to a higher one and no series is observed. It should be mentioned that in exciting the Rydberg electron from the A state ($n = 3$) to higher n-states, the radius of the Rydberg orbital becomes larger than the relaxed cage radius. The assignments were made by comparing the energy splittings observed in the fluorescence depletion spectra with the energy splittings in the gas phase, this within and between ($n\ell\lambda$) Rydberg complexes. It is found that for a given n, the s–p splittings are conserved within a factor of 2 but the s–d splittings are strongly reduced. Furthermore, the n–$(n+1)$ splittings are strongly reduced, reflecting the compression of the Rydberg series. The ionisation potential is lowered, in agreement with estimates based on the electron affinity and ion polarisation energy in the various solids. The spectra can be fitted with a Rydberg modified formula with either the quantum defect or the effective Rydberg constant as adjustable parameters. However it is stressed that these are purely phenomenological approaches, which call for a sound theoretical modelling to understand the physical meaning of the adjusted parameters. Finally, Rydberg-Rydberg transitions are observed in the case of red sites. In Ar, the data is interpreted in terms of an NO–Ar_n complex with features close to those of the NO–Ar complex.

This work was partly supported by the SNSF *via* contract 53811.98. The authors would like to thank the referees for their valuable comments.

References

1. M.B. Robin, *Higher Excited States of Polyatomic Molecules* (Academic Press, New York, 1971).
2. M. Miladi, J.-P. Le Falher, J.-Y. Roncin, H. Damany, J. Mol. Spec. **65**, 81 (1975).
3. M. Miladi, J.-Y. Roncin, H. Damany, J. Mol. Spec. **69**, 260 (1978).
4. J. Meyer, R. Reininger, U. Asaf, Chem. Phys. Lett. **173**, 384 (1990).
5. E. Morikawa, A.M. Köhler, R. Reininger, V. Saile, P. Laporte, J. Chem. Phys. **89**, 2729 (1988).
6. R. Reininger, E. Morikawa, V. Saile, Chem. Phys. Lett. **159**, 276 (1989); A.M. Köhler, R. Reininger, V. Saile, G. Findley, Phys. Rev. A **33**, 771 (1986).
7. J. Meyer, R. Reininger, U. Asaf, I.T. Steinberger, J. Chem. Phys. **94**, 1820 (1991) and references therein.
8. R. Reininger, E. Morikawa, V. Saile, Chem. Phys. Lett. **159**, 276 (1989) and references therein.
9. R. Reininger, V. Saile, *Proceedings of the XIth Molecular Crystal Symposium*, Lugano, 1985.
10. T.W. Scott, A.C. Albrecht, J. Chem. Phys. **74**, 3807 (1981).
11. N. Schwentner, J. Jortner, E.E. Koch, *Electronic Excitations in Condensed Rare Gases*, Springer Tracts in Modern Physics (Springer, Berlin, 1985).
12. M. Chergui, N. Schwentner, W. Böhmer, J. Chem. Phys. **85**, 2472 (1986).
13. W. Böhmer, R. Haensel, N. Schwentner, E. Boursey, M. Chergui, Chem. Phys. Lett. **91**, 66 (1982).
14. M. Chergui, N. Schwentner, V. Stepanenko, Chem. Phys. **187**, 153 (1994).
15. K.-H. Gödderz, N. Schwentner, M. Chergui, Chem. Phys. **209**, 91 (1996).
16. A. Gedanken, B. Raz, J. Jortner, J. Chem. Phys. **59**, 2752 (1973).
17. J. Jortner, in *VUV Radiation Physics*, edited by E.E. Koch, R. Haensel, C. Kunz (Pergamon, Oxford, 1974), p. 263.
18. J.C. Angus, G.C. Morris, Mol. Cryst. Liq. Cryst. **11**, 257; *ibid.* 309 (1970).
19. J.Y. Roncin, N. Damany, B. Vodar, Chem. Phys. Lett. **3**, 197 (1969).
20. J. Goodman, L.E. Brus, J. Chem. Phys. **67**, 933 (1977).
21. M. Chergui, N. Schwentner, V. Chandrasekharan, J. Chem. Phys. **89**, 1277 (1988).
22. N. Schwentner, M. Chergui, J. Chem. Phys. **85**, 3458 (1986) and references therein.
23. F. Vigliotti, M. Chergui, M. Dickgiesser, N. Schwentner, Faraday Disc. **108**, 139 (1997).
24. J. Wörmer, R. Karnbach, M. Joppien, T. Möller, J. Chem. Phys. **104**, 8269 (1996).
25. O. Björneholm, F. Federmann, F. Fösing, T. Möller, Phys. Rev. Lett. **74**, 3017 (1995).
26. O. Björneholm, F. Federmann, F. Fösing, T. Möller, S. Stampfli, J. Chem. Phys. **104**, 1876 (1996).
27. M. Lengen, M. Joppien, R. Pietrowski, T. Möller, Chem. Phys. Lett. **229**, 362 (1994).
28. M. Chergui, N. Schwentner, A. Tramer, Chem. Phys. Lett. **201**, 187 (1993).
29. J. Hermanson, J.C. Phillips, Phys. Rev. **150**, 652 (1966).
30. M.-C. Castex, E. Boursey, V. Chandrasekharan, Phys. Rev. B **16**, 2858, (1977).
31. K. Dressler, *Extrait des Mémoires de la Société Royale des Sciences de Liège* (Liège, 1970), Vol. XX, p. 357.
32. L. Resca, R. Resta, Phys. Rev. B **19**, 1683 (1979).
33. M. Gross, F. Spiegelmann, Eur. Phys. J. D **4**, 219 (1998).
34. G. Zerza, F. Vigliotti, A. Sassara, M. Chergui, V. Stepanenko, Chem. Phys. Lett. **256**, 63 (1996).
35. K. Sato, Y. Achiba, K. Kimura, J. Chem. Phys. **81**, 57 (1984).
36. J.C. Miller, J. Chem. Phys. **90**, 4031 (1989).
37. J. Fleniken, Y. Kim, H. Meyer, J. Chem. Phys. **109**, 8940 (1998).
38. N. Shafizadeh, P. Bréchignac, M. Dyndgaart, J.H. Fillion, D. Gauyacq, B. Lévy, J.C. Miller, T. Pino, M. Raoult, J. Chem. Phys. **108**, 9313 (1998) and references therein.
39. F. Vigliotti, M. Chergui, Chem. Phys. Lett. **296**, 316 (1998); *ibid.* **305**, 187 (1999).
40. F. Vigliotti, G. Zerza, M. Chergui, J. Rubayo-Soneira, J. Chem. Phys. **109**, 3508 (1998).
41. Y. Anezaki, T. Ebata, N. Mikami, M. Ito, Chem. Phys. **97**, 153 (1985).
42. W.Y. Cheung, W.A. Chupka, S.D. Colson, D. Gauyacq, P. Avouris, J. Wayne, J. Phys. Chem. **90**, 1086 (1986) and references therein.
43. E. Miescher, K. Huber, *Int. Review of Science, Physical Chemistry* (Butterwoth, London, 1978), Vol. 3, p. 37.
44. C. Jungen, J. Chem. Phys. **53**, 4168 (1970).
45. M. Chergui, N. Schwentner, V. Chandrasekharan, J. Chem. Phys. **89**, 7094 (1988).
46. T.F. Gallagher, *Rydberg atoms* (Cambridge University Press, 1994).
47. I. Fouré, M. Raoult, Chem. Phys. **198**, 1 (1995).
48. K. Onda, K. Yamanouchi, J. Chem. Phys. **102**, 1129 (1995).
49. B.G. Brunetti, F. Vecchiocattivi, in *Cluster Ions*, edited by C.Y. Ng, T. Baer, I. Powis (John Wiley and Sons Ltd, 1993).
50. R.H. Lipson, R.W. Field, J. Chem. Phys. **110**, 10653 (1999).
51. E. Fermi, Nuovo Cimento **11**, 157 (1934).
52. H.S.W. Massey, E.H.S. Burhop, *Electronic and Impact Phenomena* (Oxford University Press 1952), p. 178.
53. V.A. Alekseev, I.I. Sobel'man, Sov. Phys. JETP **22**, 882 (1966).
54. I.I. Sobel'man, L.A. Vainshtein, E.A. Yukov, *Excitation of Atoms and Broadening of Spectral Lines* (Springer-Verlag, Berlin, 1981), Chap. 7.
55. I. Fouré, Ph.D. thesis, University Paris-Sud, 1994.